Research Article | Vol. 30, No. 20 / 26 Sep 2022 / Optics Express 35749
Optics EXPRESS

Graphene-enhanced hybrid terahertz metasurface sensor for ultrasensitive nortriptyline sensing and detection

KAI SUN,[1,2] JINING LI,[1,2,3,*] LIANG GE,[1,2] KAI ZHONG,[1,2] YUYE WANG,[1,2] DEGANG XU,[1,2,3] XIANG YANG,[4] WEILING FU,[4] AND JIANQUAN YAO[1,2]

[1]*Institute of Laser and Optoelectronics, School of Precision Instruments and Opto-Electronics Engineering, Tianjin University, Tianjin 300072, China*
[2]*Key Laboratory of Opto-Electronic Information Technology, Ministry of Education, Tianjin University, Tianjin 300072, China*
[3]*Key Laboratory of Micro Opto-electro Mechanical System Technology, Tianjin University, Ministry of Education, Tianjin 300072, China*
[4]*Department of Laboratory Medicine, Southwest Hospital, Third Military Medical University (Army Medical University), Chongqing 400038, China*
[*]*jiningli@tju.edu.cn*

Abstract: Graphene is a two-dimensional material with unique physical and chemical properties, whose excellent biocompatibility has also attracted widespread attention in the field of biosensing and medical detection. Graphene provides a novel solution for dramatically improving the sensitivity of terahertz metasurface sensors, since the electrical conductivity can be modified by contact with biomolecules. In this paper, a metal-graphene hybrid metasurface is proposed and demonstrated for high-sensitive nortriptyline sensing based on the plasmon-induced transparency (PIT) resonances. The π-π stacks between nortriptyline and graphene lead to an increase in the Fermi level of graphene and a decrease in the conductivity, thus enhancing the PIT resonance. Experimental results show that the peak-to-peak amplitude magnitude of the PIT window is enhanced up to 3.4-fold with 1 ng nortriptyline analyte, and the minimum detection limit is extended down to 0.1 ng. But no significant change is observed from the samples without graphene as a comparative experiment, which demonstrates that the presence of graphene greatly enhances the bonding to the drug molecules and improves the sensing sensitivity. This metasurface sensor has the advantages of high sensitivity, fast detection speed, label-free and steady properties, which has potential applications in the fields of trace molecular sensing and disease diagnosis.

1. Introduction

Metasurfaces, realized by artificial subwavelength unit cell structures, are able to manipulate the polarization, amplitude, and phase of electromagnetic (EM) waves by changing the geometry of the unit cell structure and thus enable the versatile functionalities [1–4]. In recent years, the in-depth investigation of metasurfaces for terahertz (THz) band has promoted the development and the application of THz technology, fulfilling the THz gap to a great extent, such as absorbers [5,6], filters [7], polarization converters [8,9], sensors [10], lenses [11], etc. The manipulation of EM waves by metasurfaces is achieved through resonance generated by artificial unit structures whose surface local EM field is sensitive to surface substances on the top, making the metasurfaces desirable for sensing applications. For example, in 2016, Qin et al. proposed a metamaterial sensor with circular pore arrays and used it for sensing tetracycline hydrochloride with a detection limit as low as 0.1 μg/ml [12]. In 2018, Yang et al. proposed a metasurface sensor based

#470772 https://doi.org/10.1364/OE.470772
Journal © 2022 Received 17 Jul 2022; revised 22 Aug 2022; accepted 5 Sep 2022; published 15 Sep 2022

Optics EXPRESS

on a gold split-ring resonator to achieve efficient label-free discrimination between wild-type and transgenomic DNA with a detection limit as low as 2.3 μg/ml [13]. In 2022, Lee et al. distinguished the spike protein of aevere acute respiratory syndrome coronavirus 1 and 2 at a concentration of 0.1 mg/ml using a metal slit array metasurface sensor [14]. High-sensitivity metasurface sensors facilitate the detection of various disease markers, which is also the current trend of the sensor. However, the spectra of metasurface sensors contain at least one sharp resonance peak, which is difficult to achieve due to the limited processing accuracy. Frequency shifts in the spectrum due to the changes of the dielectric environment induced by the analyte are commonly employed as the sensing method, which means that this type of sensor requires a certain amount of analyte to be deposited on the surface and has difficulty in achieving ultra-high sensitivity.

To overcome the difficulty of ultra-high sensitivity of sensors based on the frequency shift principle, we combine graphene and plasmon-induced transparency (PIT) metasurfaces to achieve sensing based on transmission spectrum amplitude changes. Graphene is a two-dimensional material consisting of a single layer of carbon atoms with unique electrical, optical, thermal and mechanical properties, which has received great attention in materialogy, electromagnetism, electrochemistry and so on [15–17]. Owing to the presence of π-electrons, graphene has a great affinity for biomolecules and has excellent potential for sensing small and organic macromolecules [18]. Therefore, introducing graphene into the metasurface is expected to improve the sensitivity of metasurface sensors to a great extent. For example, in 2019, Xu et al. detected chlorpyrifos-methyl molecules by transferring a single layer of graphene on the surface of a THz absorber composed of a square metal patch array and comparing changes in the magnitude of absorption [19]. In 2020, Lee et al. reported that the low concentrations (~nmol/μl) of single-stranded deoxyribonucleic acids could be detected using transmission magnitude variations of graphene-combined nano-slot-based THz resonance [20]. All these metasurface sensors are sensing strategies based on amplitude changes in transmission or reflection of a single resonant peak and are susceptible to the instability of the detection instrument. PIT, which mimics the classical quantum electromagnetic-induced transparency (EIT) phenomenon, is an effective strategy to control the transmission properties of terahertz waves [21,22]. Due to the strong interference between different resonance modes, a transparent sharp peak in the spectrum of the PIT metasurfaces, as called as the PIT window, is more suitable for amplitude change sensing than frequency shift sensing. Therefore, PIT metasurfaces in combination with graphene are expected to achieve more sensitive and stable sensing compared to classical single resonant metasurfaces.

Various psychiatric disorders such as depression, anxiety disorders and bipolar disorder are a category of easily neglected diseases that endanger people's health and can most seriously cause suicide. Nortriptyline (3-(10,11-dihydro-5H-dibenzo (a,b) cyclohepten-5-ylidene) propyl-(methyl) amine) is a tricyclic antidepressant for the treatment of these psychiatric disorders [23]. The therapeutic concentration range of nortriptyline in human plasma is between 50 and 150 ng/mL [24]. To achieve optimal treatment results, it is necessary to ensure that the concentration of nortriptyline is within its therapeutic range. Currently, high-performance liquid chromatography, spectrophotometry, fluorescence spectrophotometry and potentiometric methods are used to test the concentration of nortriptyline, but all of these methods require at least tens of minutes [24]. Therefore, a fast, label-free and sensitive sensing of nortriptyline is necessary.

In this paper, a metal-graphene hybrid metasurface (MGHM) sensor composed of a classical PIT metal metasurface and monolayer graphene for sensing nortriptyline is proposed and demonstrated. The interaction between graphene and nortriptyline molecules makes the sensor highly sensitive to the concentration of nortriptyline. Theoretical analysis and simulation verification explain the operating mechanism of the sensor. The experimental results indicate

Optics EXPRESS

that the ultra-low quantity of nortriptyline is able to significantly enhance the PIT window of the MGHM transmission spectrum, compared with the PIT metasurface without graphene. The fast, label-free, and steady under the test system disturbance characteristics enable it an excellent potential in the field of biomolecular sensing and disease detection.

2. Design, fabrication, and characterization of the hybrid metasurface

The design of the MGHM we proposed is illustrated in Fig. 1(a), which consists of a PIT metal-insulator metasurface (MM) with a monolayer of graphene on the top. The PIT MM consists of a silicon substrate, a silicon dioxide layer and a gold resonator layer, with thicknesses of 500 μm, 300 nm, 200 nm, respectively. The PIT resonator unit cell is composed of a metal cut wire (CW) and two pairs of spilt-ring resonators (SRRs) on both sides with the specific geometries as shown in Fig. 1(b), where P = 80 μm, L_1 = 25 μm, L_2 = 70 μm, D = 7 μm, G = 5 μm, W = 5 μm.

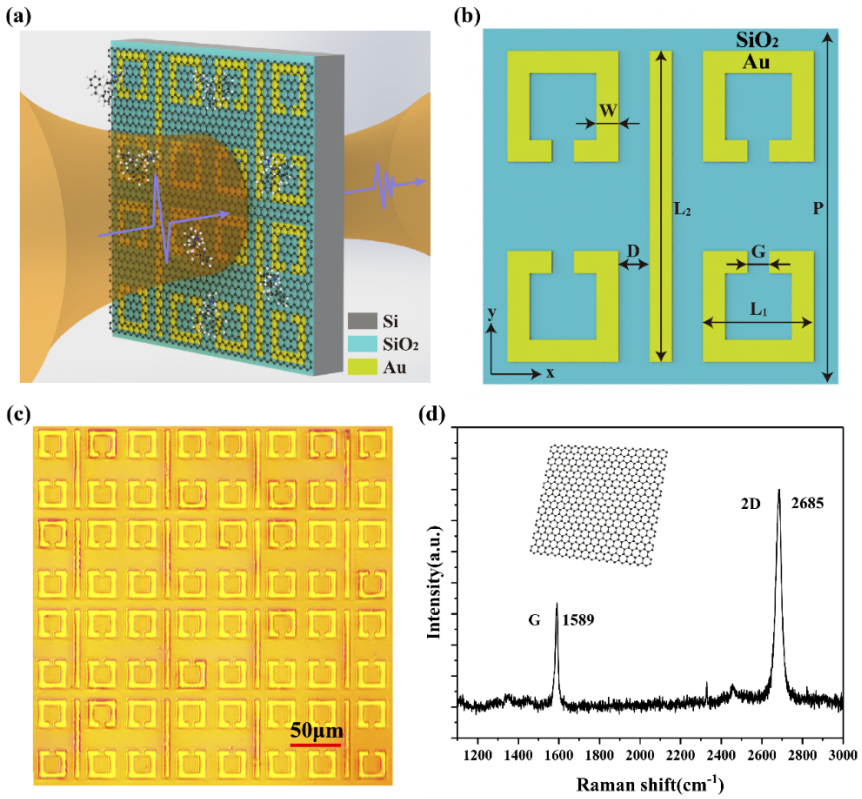

Fig. 1. (a) Schematic diagram of sensing process on MGHM sensor. (b) Schematic of unit cell of PIT structure. (c) Optical microscope photograph of MGHM sample. (d) Raman spectroscopy of graphene on the hybrid metasurface.

The fabrication process of the MGHM sensor started with the growth of a 300 nm thick SiO_2 layer on 500um of n-type high resistance silicon by plasmon-enhanced chemical vapor deposition (PECVD). Subsequently, a 20/200 nm thick Cr/Au spacer was magnetron sputtered on top and was patterned using standard photolithography and ion beam etching methods. Finally, monolayer graphene prepared by chemical vapor deposition (CVD) was transferred to the surface. Figure 1(c) shows the optical microscope photograph of the fabricated MGHM sample. However, the graphene layer is barely visible in the photograph. In order to make sure the successful

Optics EXPRESS

transfer of graphene on the surface of MGHM, Raman spectroscopy (Renishaw inVia Reflex) with 532 nm laser excitation is used for characterization. As shown in Fig. 1(d), the single Lorentzian shape of low-intensity G-peak (~1589 cm^{-1}) and high-intensity 2D-peak (~2685 cm^{-1}), as well as the absence of D-peak (~1340 cm^{-1}), demonstrate the high-quality of monolayer graphene on the top of the MGHM.

3. Theoretical model and simulation analysis

In order to effectively investigate the electromagnetic responses of the MGHM, the simulations are performed by the time domain solver of CST Microwave Studio software. Periodic boundary conditions are employed in x- and y-direction and open boundary condition is employed in z-direction. The incident THz wave is simulated as a linearly polarized wave along the y-direction generated from a plane wave excitation and the transmitted wave from the metasurface is detected by a probe. The relative permittivity of Si and SiO_2 is set as 11.7 and 3.84, and the conductivity of Au is set to 4.56×10^7 S/m, respectively [20,25,26]. In order to illustrate the bright and dark resonance modes in PIT, three sets of structures are simulated for comparison. Figures 2(a)-(c) and 2(d)-(g) are the simulated transmission spectra and the corresponding surface electric field distributions at the resonance frequency, respectively. The first structure is a single metal CW along the y-direction. Excited by the incident THz wave with the linearly polarized (LP) along the y-direction, CW exhibits a typical dipole resonance mode with a wide resonance at 0.818 THz, as shown in Figs. 2(a) and 2(d). The second structure is two pairs of symmetrical SRRs. As shown in Figs. 2(b) and 2(e),(f), SRRs exhibit two different electromagnetic responses under the excitation of LP waves in different directions. It is obvious that no resonance has been excited by the LP wave along the y-direction (purple solid line). And LP wave along the x-direction (parallel to the split-ring direction) excites a narrow resonance with the inductive-capacitive (LC) mode at 0.812 THz (red solid line). The third is the PIT structure composed of a CW and four SRRs. As shown in Fig. 2(c), a transparent window is clearly observed at 0.812 THz on the transmission spectrum with the incident LP wave along the y-direction. In this structure, the dipole resonance from the CW directly excited by the incident wave acts as the bright mode, while the LC resonance from the SRRs excited by the near-field coupling between the CW and the SRRs acts as the dark mode, as shown in Fig. 2(g). The destructive interference between the bright and dark modes leads to the PIT window.

In the literature, graphene is generally simulated using the well-known Kubo conductivity model [26–28]:

$$\begin{aligned}\sigma_g(\omega, E_F, \tau, T) &= \sigma_{inter} + \sigma_{intra} \\ &= \frac{je^2(\omega - j\tau^{-1})}{\pi\hbar^2} \times \left[\frac{1}{(\omega - j\tau^{-1})^2} \int_0^\infty \frac{\partial f_d(\varepsilon)}{\partial \varepsilon} - \frac{\partial f_d(-\varepsilon)}{\partial \varepsilon} d\varepsilon - \int_0^\infty \frac{f_d(-\varepsilon) - f_d(\varepsilon)}{(\omega - j\tau^{-1})^2 - 4(\varepsilon/\hbar)^2} d\varepsilon \right],\end{aligned} \tag{1}$$

where f_d is the Fermi-Dirac distribution, T is the operation temperature, $\hbar$ is the reduced Planck constant, ω is the angular frequency of the incident wave, e is the charge of an electron, and E_F is the Fermi level, which is determined by the carrier concentration. $\tau = (\mu E_F)/(ev_F^2)$ denotes the carrier relaxation time, where μ=8000 $cm^2/(V \cdot s)$ is the carrier mobility, $v_F = 10^6$ m/s is the Fermi velocity. In the Kubo model, the graphene conductivity includes both intraband and interband processes, while in the low-frequency terahertz region, the contribution of interband processes is negligible. And the doped graphene at room temperature satisfies $E_F \gg K_B T$ (K_B is the Boltzmann constant) and $E_F \gg \hbar\omega$. Therefore, the Eq. (1) can be reduced to the following Drude-like model [28,29]:

$$\sigma_g = \frac{e^2 E_F}{\pi\hbar^2} \frac{i}{\omega + i\tau^{-1}}. \tag{2}$$

Optics EXPRESS

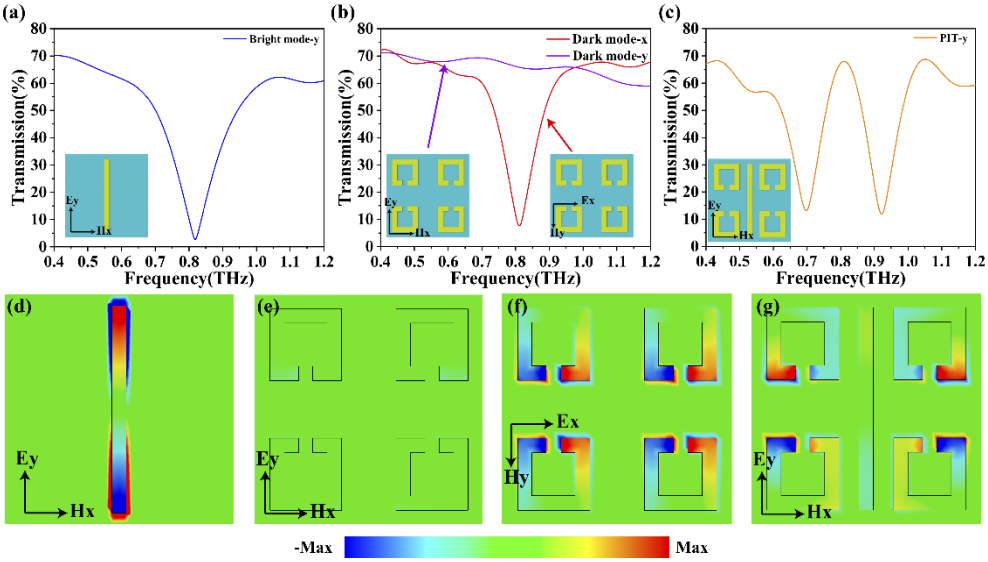

Fig. 2. Simulated transmission spectra of (a) CW, (b) SRRs, and (c) PIT structures. Simulated surface electric field distribution of (d) CW, (e) SRRs for incident LP THz wave along the y-direction, (f) SRRs for incident LP THz wave along the x-direction, and (g) PIT structures.

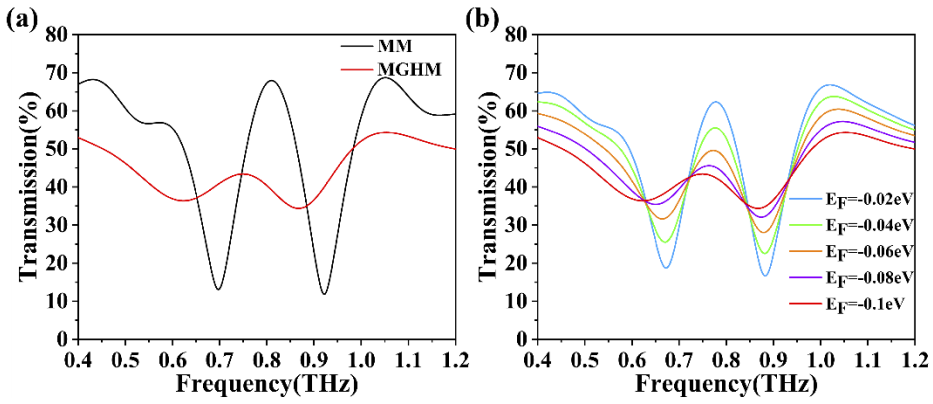

Fig. 3. (a) Simulated transmission spectra of MM and MGHM with Fermi level of graphene at -0.1eV. (b) Simulated transmission spectra of MGHM with different Fermi level of graphene.

Optics EXPRESS

Obviously, the conductivity of graphene is modulated by the Fermi level. After a 0.35 nm thick graphene layer is added on the top of MM in the simulation, the comparison of transmission spectra of MM and MGHM with Fermi level of graphene at -0.1 eV are shown in Fig. 3(a). The graphene on the top weakens the bright resonance mode and the near-field coupling between bright and dark resonance modes resulting in a significant shrinkage of the PIT window. And the center frequency of the PIT peak of MGHM is 0.750 THz, which has a significant redshift for the transmission spectrum of MGHM compared with MM. When the sensing substance is in contact with graphene, the Fermi level of graphene shifts upward and converges to the Dirac point. Therefore, the transmission spectra of MGHM of graphene Fermi level from -0.1 to -0.02 were simulated and analyzed as shown in Fig. 3(b). With the Fermi level gradually moving towards the Dirac point, the conductivity of graphene gradually decreases and the PIT window of the transmission spectrum gradually enhances.

4. Experiment results of sample measurement and nortriptyline sensing

The transmission spectra of MGHM and MM samples are measured by THz time-domain spectroscopy (THz-TDS, TAS 7500TS, Advantest Corp.), as shown in Fig. 4(a). It can be seen that an obvious PIT window is present in the transmission spectrum of MM. However, when the graphene layer is transferred to the MM surface, the surface local electromagnetic field of the metasurface is affected because graphene is a conductive medium. The PIT window of MGHM is significantly shrunk and the center frequency has a redshift from 0.875 THz to 0.833 THz. The difference between the maximum and minimum values of the transmission of the PIT peak and valley is defined as ΔT, which is used as the sensing index of the sensor. The change in ΔT reflects the relationship between the quantity of nortriptyline and the variation of the Fermi level of graphene. The increase of ΔT means that the Fermi level of graphene tends to move toward the Dirac point and conversely, away from the Dirac point. Because the p-type doping resulting from the contact of graphene with SiO_2 substrate, gold patterns, and oxygen makes the Fermi level of intrinsic graphene deviate from the Dirac point into the valence band, causing the significant shrinking of the PIT window [30–32]. Here, ΔT shrinks from 55.2% to 6.4%.

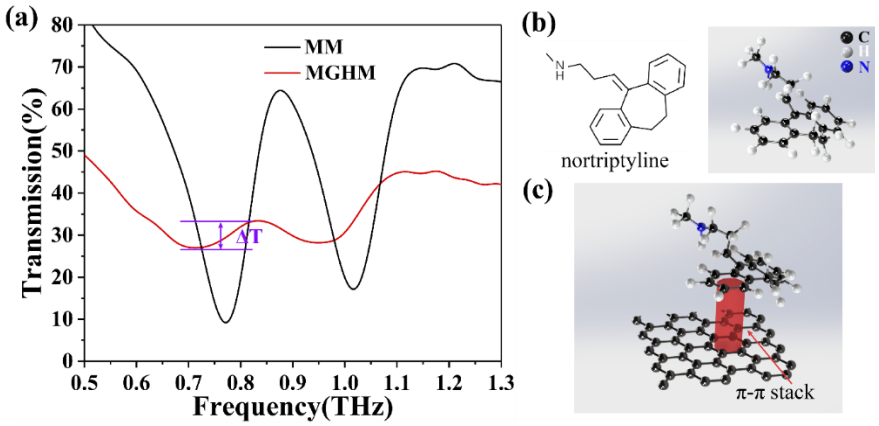

Fig. 4. (a) The transmission spectra of MGHM and MM sensor. (b) The molecular skeletal formula and molecular structural diagram of nortriptyline. (c) Schematic diagram of the π-π stack between graphene and nortriptyline

In this paper, the MGHM sensor is used for sensing of nortriptyline hydrochloride (purchased from Acmec, Shanghai, purity ≥98%). The nortriptyline is dissolved in deionized water to configure solutions with a concentration of 10 ng/ml. Each time 10ul solution of nortriptyline is

Optics EXPRESS

added dropwise to the surface of the MGHM sensor and the MM senso and wait until the water in the solution is completely evaporated under the condition of a 70°C heating platform, implying that 0.1ng nortriptyline is deposited on the surface. In total, 10 times have been repeated to prepare and measure the analytes by THz-TDS with different quantities of nortriptyline from 0 to 1 ng, respectively.

The transmission spectra of the MGHM sensor and MM sensor with different quantities of nortriptyline deposited on the surface are shown in Figs. 5(a) and 5(b). It can be obviously observed that for the MGHM sensor, the PIT window is significantly enhanced with the increase of nortriptyline. However, for the MM sensor, the PIT window rarely changes. To facilitate direct observation of the effect of nortriptyline on the PIT window, the ΔT of MGHM corresponding to nortriptyline deposited from 0.1 ng to 1 ng are shown in Fig. 5(c) and fitted with an exponential function $y = y_0 + a_1 e^{-x/t_1}$, where $y_0 = 22.8618$, A_1=-16.2855, $t_1 = 0.3628$, respectively. When the lower quantities of the nortriptyline are deposited on the MGHM surface, ΔT grows rapidly. But as the quantities increases, the growth rate of ΔT gradually slows down and tends to saturate. With 1 ng of nortriptyline deposited on the surface, ΔT has been enhanced to 21.9%, which is approximately 3.4 times higher than that of bare MGHM. The detection limit of the experimental measurement for nortriptyline is as low as 0.1 ng with ΔT enhanced up to 10.2%.

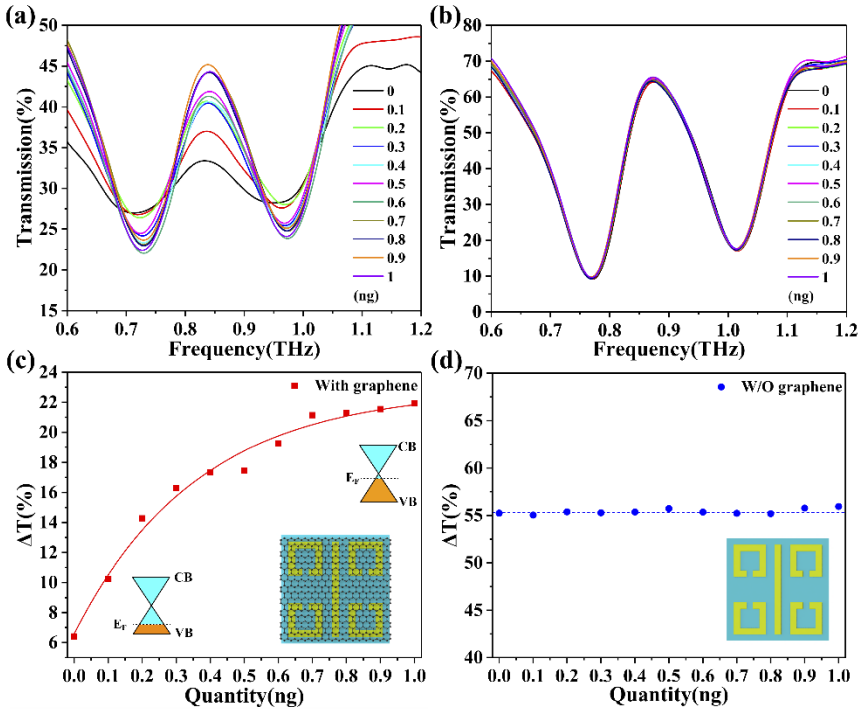

Fig. 5. Experimental transmission spectra of (a) MGHM sensor and (b) MM sensor with different quantities of nortriptyline deposited on the surface. (c) ΔT values and fitted curve of MGHM sensor. (d) ΔT values and fitted straight line of MM sensor. The insets are the diagrams of the unit cells of sensors and the energy band with the Fermi level shifting, in which VB is the valence band and the CB is the conduction band.

The variation in optical properties of graphene is attributed to the interaction with external molecules. The three electrons of each carbon atom of graphene are bonded by sp^2 hybridization orbitals, and the remaining one electron forms a π-bond. As shown in Figs. 4(b) and 4(c), nortriptyline containing two phenyl rings carry π-electrons and form π-π stacks with graphene,

Optics EXPRESS

which have strong interactions and charge transfer. The interaction with nortriptyline results in n-type doping of graphene, which also induces an increase in the electron concentration of graphene and a rise of the Fermi level. And the quantity of nortriptyline gradually increased from 0.1 ng to 1 ng, so that the Fermi energy level gradually shifts upward and tends to the dirac point. With the Fermi level approaching the Dirac point, the conductivity of graphene decreases, which enhances the dipole resonance, the near-field coupling interaction and the destructive interference between the dipole resonance of CWs and the LC resonance of SRRs, therefore leading to the enhancement of the PIT window in the transmission spectrum. The same variation rules of simulation and experimental results prove the consistency of theory and experiment. In contrast, for the MM sensor, 1 ng of nortriptyline has no significant effect on its surface EM field, and the ΔT keeps staying around 55.3%, as shown in Fig. 5(d). Thus, the presence of graphene enables a tremendous improvement in sensing sensitivity. The MGHM sensor we proposed has an outstanding high detection sensitivity for nortriptyline and satisfies the needs for sensing and monitoring plasma concentrations in clinical medicine. Furthermore, the potential influences from the instability of the measurement system are attenuated to a great extent, because the sensing index is the transmittance difference between the PIT peak and valley, which is an advantage of the PIT structure [19,20,33,34].

5. Conclusion

In this paper, an MGHM sensor with ultra-high sensitivity and stability based on PIT metasurface structure is proposed and demonstrated as a biosensing platform for nortriptyline microdose detection. The design of the metal-graphene hybrid structure in unit cell greatly improves the sensing sensitivity, because the biomolecules of the analyte are concentrated on the graphene by bonding π-π stacks, while the metal PIT metasurface structure provides the strong resonance of surface plasmonic polaritons with enough resonant intensity for sensing. The interaction and charge transfer between nortriptyline and graphene adjusts the Fermi level, modifies the conductivity of graphene, and indeed modulates the amplitude magnitude of the PIT resonance. The experimental results show that the peak-to-peak amplitude magnitude of the PIT resonance, i.e., the ΔT, increases from 6.4% to a maximum of 21.9% with nortriptyline increasing from 0 to 1 ng, implying that 1 ng nortriptyline enhanced the PIT window up to 3.4-fold compared to the blank MGHM. And the detection limit is extended down to 0.1 ng. The sensing sensitivity of MGHM appears to be significantly improved compared to the bare MM without graphene, demonstrating the vital role of graphene for improving sensing sensitivity. This rapid, label-free, high-efficient MGHM sensor satisfies the requirements for plasma concentration detection of nortriptyline in clinical applications. This sensor has an outstanding prospect for applications in ultra-low concentration biomolecule sensing, disease diagnosis, DNA and protein sequencing, etc.

Funding. National Natural Science Foundation of China (61705162).

Acknowledgments. The authors sincerely thank the advice given by Pan Wang (Capital Medical University) and Key Laboratory of Opto-electronic Information Technology and Key Laboratory of Micro Opto-electro Mechanical System Technology, Tianjin University, Ministry of Education, Tianjin, 300072, P. R. China.

Disclosures. The authors declare no conflicts of interest.

Data availability. Data underlying the results presented in this paper are not publicly available at this time but may be obtained from the authors upon reasonable request.

References

1. M. Gupta, Y. K. Srivastava, M. Manjappa, and R. Singh, "Sensing with toroidal metamaterial," Appl. Phys. Lett. **110**(12), 121108 (2017).
2. C. Huang, Y. Feng, J. Zhao, Z. Wang, and T. Jiang, "Asymmetric electromagnetic wave transmission of linear polarization via polarization conversion through chiral metamaterial structures," Phys. Rev. B: Condens. Matter Mater. Phys. **85**(19), 195131 (2012).

Optics EXPRESS

3. C. Zhang, Q. Cheng, J. Yang, J. Zhao, and T. J. Cui, "Broadband metamaterial for optical transparency and microwave absorption," Appl. Phys. Lett. **110**(14), 143511 (2017).
4. R. Zhu, X. N. Liu, G. K. Hu, C. T. Sun, and G. L. Huang, "Negative refraction of elastic waves at the deep-subwavelength scale in a single-phase metamaterial," Nat. Commun. **5**(1), 5510 (2014).
5. J. Huang, J. Li, Y. Yang, J. Li, J. Li, Y. Zhang, and J. Yao, "Broadband terahertz absorber with a flexible, reconfigurable performance based on hybrid-patterned vanadium dioxide metasurfaces," Opt. Express **28**(12), 17832 (2020).
6. F. Ding, S. Zhong, and S. I. Bozhevolnyi, "Vanadium Dioxide Integrated Metasurfaces with Switchable Functionalities at Terahertz Frequencies," Adv. Opt. Mater. **6**(9), 1701204 (2018).
7. N. Born, M. Reuter, M. Koch, and M. Scheller, "High-Q Terahertz Bandpass Filters Based on Coherently Interfering Metasurface Reflections," Opt. Lett. **38**(6), 908 (2013).
8. R. T. Ako, W. S. L. Lee, S. Atakaramians, M. Bhaskaran, S. Sriram, and W. Withayachumnankul, "Ultra-wideband tri-layer transmissive linear polarization converter for terahertz waves," APL Photonics **5**(4), 046101 (2020).
9. R. M. H. Bilal, M. A. Baqir, P. K. Choudhury, M. M. Ali, and A. A. Rahim, "On the specially designed fractal metasurface-based dual-polarization converter in the THz regime," Results Phys. **19**, 103358 (2020).
10. M. S. Islam, J. Sultana, M. Biabanifard, Z. Vafapour, M. J. Nine, A. Dinovitser, C. M. B. Cordeiro, B. W. H. Ng, and D. Abbott, "Tunable localized surface plasmon graphene metasurface for multiband superabsorption and terahertz sensing," Carbon **158**, 559–567 (2020).
11. N. Kundtz and D. R. Smith, "Extreme-angle broadband metamaterial lens," Nat. Mater. **9**(2), 129–132 (2010).
12. J. Qin, L. Xie, and Y. Ying, "A high-sensitivity terahertz spectroscopy technology for tetracycline hydrochloride detection using metamaterials," Food Chem. **211**, 300–305 (2016).
13. Y. Yang, D. Xu, and W. Zhang, "High-sensitivity and label-free identification of a transgenic genome using a terahertz meta-biosensor," Opt. Express **26**(24), 31589 (2018).
14. S. H. Lee, Y. K. Lee, S. H. Lee, J. Kwak, H. S. Song, and M. Seo, "Detection and discrimination of SARS-CoV-2 spike protein-derived peptides using THz metamaterials," Biosens. Bioelectron. **202**, 113981 (2022).
15. K. S. Novoselov, V. I. Fal'Ko, L. Colombo, P. R. Gellert, M. G. Schwab, and K. Kim, "A roadmap for graphene," Nature **490**(7419), 192–200 (2012).
16. M. Liu, X. Yin, E. Ulin-Avila, B. Geng, T. Zentgraf, L. Ju, F. Wang, and X. Zhang, "A graphene-based broadband optical modulator," Nature **474**(7349), 64–67 (2011).
17. A. T. Lawal, "Graphene-based nano composites and their applications. A review," Biosens. Bioelectron. **141**, 111384 (2019).
18. S. Farid, X. Meshik, M. Choi, S. Mukherjee, Y. Lan, D. Parikh, S. Poduri, U. Baterdene, C. E. Huang, Y. Y. Wang, P. Burke, M. Dutta, and M. A. Stroscio, "Detection of Interferon gamma using graphene and aptamer based FET-like electrochemical biosensor," Biosens. Bioelectron. **71**, 294–299 (2015).
19. W. Xu, L. Xie, J. Zhu, L. Tang, R. Singh, C. Wang, Y. Ma, H. T. Chen, and Y. Ying, "Terahertz biosensing with a graphene-metamaterial heterostructure platform," Carbon **141**, 247–252 (2019).
20. S. H. Lee, J. H. Choe, C. Kim, S. Bae, J. S. Kim, Q. H. Park, and M. Seo, "Graphene assisted terahertz metamaterials for sensitive bio-sensing," Sens. Actuators, B **310**, 127841 (2020).
21. Y. Yang, J. Li, J. Li, J. Huang, Q. Li, Y. Zhang, H. Dai, and J. Yao, "Optical control of terahertz plasmon-induced transparency based on hybrid CsPbBr 3 quantum dot metasurfaces," Opt. Express **28**(16), 24047 (2020).
22. X. Yan, M. Yang, Z. Zhang, L. Liang, D. Wei, M. Wang, M. Zhang, T. Wang, L. Liu, J. Xie, and J. Yao, "The terahertz electromagnetically induced transparency-like metamaterials for sensitive biosensors in the detection of cancer cells," Biosens. Bioelectron. **126**, 485–492 (2019).
23. A. Nezhadali, Z. Mehrdadian, and M. Mojarrab, "Nanogram/mL detection of nortriptyline: Preparation of a molecularly imprinted polymer for spectrophotometric determination of nortriptyline based on multivariate optimization methods," J. Sep. Sci. **42**(22), 3479–3486 (2019).
24. M. Guzinski, E. Lindner, B. Pendley, and E. Chaum, "Electrochemical sensor for tricyclic antidepressants with low nanomolar detection limit: Quantitative Determination of Amitriptyline and Nortriptyline in blood," Talanta **239**, 123072 (2022).
25. M. Zhang and Z. Song, "Terahertz bifunctional absorber based on a graphene-spacer-vanadium dioxide-spacer-metal configuration," Opt. Express **28**(8), 11780 (2020).
26. S. Xiao, T. Wang, T. Liu, X. Yan, Z. Li, and C. Xu, "Active modulation of electromagnetically induced transparency analogue in terahertz hybrid metal-graphene metamaterials," Carbon **126**, 271–278 (2018).
27. V. P. Gusynin, S. G. Sharapov, and J. P. Carbotte, "Magneto-optical conductivity in graphene," J. Phys.: Condens. Matter **19**(2), 026222 (2007).
28. J. Li, J. Li, Y. Yang, J. Li, Y. Zhang, L. Wu, Z. Zhang, M. Yang, C. Zheng, J. Li, J. Huang, F. Li, T. Tang, H. Dai, and J. Yao, "Metal-graphene hybrid active chiral metasurfaces for dynamic terahertz wavefront modulation and near field imaging," Carbon **163**, 34–42 (2020).
29. G. Giovannetti, P. A. Khomyakov, G. Brocks, V. M. Karpan, J. van den Brink, and P. J. Kelly, "Doping graphene with metal contacts," Phys. Rev. Lett. **101**(2), 026803 (2008).
30. Z. He, L. Li, H. Ma, L. Pu, H. Xu, Z. Yi, X. Cao, and W. Cui, "Graphene-based metasurface sensing applications in terahertz band," Results Phys. **21**, 103795 (2021).
31. Z. Zhang, H. Huang, X. Yang, and L. Zang, "Tailoring electronic properties of graphene by π-π Stacking with aromatic molecules," J. Phys. Chem. Lett. **2**(22), 2897–2905 (2011).

Optics EXPRESS

32. H. el Khatib, B. Asaad, A. Zaylaa, F. Awad, M. Sbeity, S. Mneimneh, G. Haber, Z. Naja, and M. Rajab, "Hawkinsinuria with direct hyperbilirubinemia in Egyptian-Lebanese boy," Front. Pediatr. **7**, 69 (2019).
33. R. Zhou, C. Wang, Y. Huang, K. Huang, Y. Wang, W. Xu, L. Xie, and Y. Ying, "Label-free terahertz microfluidic biosensor for sensitive DNA detection using graphene-metasurface hybrid structures," Biosens. Bioelectron. **188**, 113336 (2021).
34. L. Xu, J. Xu, W. Liu, D. Lin, J. Lei, B. Zhou, Y. Shen, and X. Deng, "Terahertz metal-graphene hybrid metamaterial for monitoring aggregation of Aβ16–22 peptides," Sens. Actuators, B **367**, 132016 (2022).